Quantitative fatigue crack evaluation in pipeline structures using nonlinear cylindrical waves

Ruiqi Guan[1], Ye Lu[1,*], Kai Wang[2], Zhongqing Su[2]

[1]*Department of Civil Engineering*
Monash University
Clayton, VIC 3800, Australia
[2] *Department of Mechanical Engineering*
The Hong Kong Polytechnic University,
Kowloon, Hong Kong SAR

[*] To whom all correspondence should be addressed

Email: *ye.lu@monash.edu* (Dr Ye LU) Fax: +61-3-9905-4944

Abstract

This study comprehensively investigated the interaction between fatigue crack propagation and cylindrical guided waves which were excited and collected by surface-mounted piezoelectric elements on an aluminium pipe to identify the wave nonlinearity induced by the fatigue crack. Numerical simulation and experimental testing were conducted to quantify the relation between the crack length and the wave nonlinearity collected in both transmission and reflection configurations using an appropriate nonlinear index, where the co-existence of flexural wave modes as a wave group at second harmonic was considered. Both numerical and experimental results revealed that the nonlinear index first increased monotonously and then it started to drop with the further growth of the crack, a phenomenon which can be utilised for quantitative assessment of initiation of fatigue cracks. Finally, the differences between the results from simulation and experiment are compared and discussed, where possible reasons for the change in nonlinear index in both approaches are elaborated.

1. Introduction

Pipelines are crucial infrastructure which suffer from various sorts of damage such as impact, corrosion and aging. Cylindrical guided waves are efficient for pipeline inspection, with the properties of long propagation range, strong robustness and high sensitivity [1]. Research work has been conducted to detect different types of gross damage [2-5] in pipes by linear wave characteristics. However, micro-scale damage such as initial fatigue crack, corrosion at early stage, and material degradation cannot be detected in some circumstances using linear wave based methods, restricted by the wavelength of the excited wave mode. On the other hand, guided waves based on nonlinear characteristics are promising in these cases, where nonlinear distortion caused by the discontinuities, such as higher harmonic generation, subharmonic generation, and mixed frequency responses, can be detected in the structure.

Applications of numerical simulation and experimental observation in terms of the nonlinearity from material and contact acoustic nonlinearity (CAN) caused by damage in metallic structures have shown great progression. Among different modelling approaches for wave and microcrack interaction [6], a "breathing" crack model has been widely utilised to explain the behaviour of a fatigue crack distorted by guided waves. To model material nonlinearity or CAN, the finite element (FE) method has generally been used to investigate the relation between nonlinear parameters and microcrack length [7] and to locate microcracks [8] in plate structures. Studies from [7] with S_0 mode excitation have shown that the nonlinear parameter increases monotonously with crack length. Time reversal method using sensing data from FE modelling has been proposed to construct close crack imaging in an aluminium plate [9]. Another simulation method known as local interaction simulation approach (LISA) provided an efficient and optimised model for the clapping phenomenon of the fatigue crack when the wave interacted with it in the plate [10]. Furthermore, LISA and Cellular Automata for Elastodynamics (CAFE) modelling were also applied in nonlinear media for analysing the

wave propagation and the differences between these two methods were compared and discussed [11].

Further experimental testing has revealed the increasing relation between the nonlinear parameter and the severity of fatigue cracks through the mixed frequency response method [12] or the second harmonic generation method [13] in aluminium specimens. Apart from metallic structures, the nonlinearity detected by higher harmonic generation method was also studied in composites for delamination [14], thermal fatigue [15] and fatigue damage [16].

So far, however, studies conducted in pipes have been most focused on material nonlinearity. Analyses through theoretical and numerical models with the consideration of higher harmonic generation have been investigated comprehensively, from arbitrary cross-sections nonlinear waveguides [17] to weakly nonlinear cylinders [18-20]. Simulation results have illustrated that the prerequisites for cumulative second harmonic generation with different mode excitation in pipe structures were synchronism and non-zero power flux. Through experimental studies, an aluminium pipe under thermal fatigue damage was evaluated by the second harmonic generation method and the accumulation of second harmonic was also observed with the increase in propagation distance [21]. Furthermore, studies using torsional waves to detect cubic material nonlinearity in a pipe have shown linearly increasing cumulative harmonic as the wave propagation distance increased [22]. Apart from using waves that propagate axially in cylinders, experiments with nonlinear circumferential guided waves have also been carried out to validate the severity evaluation of accumulated damage in tubes using the second harmonic generation method [23].

However, limited studies using CAN have been undertaken for pipe-like structures, while the relation between the severity of microcracks and the nonlinear parameter is still not well established. In particular, the existence of multiple flexural wave modes in pipe-like structures further complicates the interaction between breathing crack and waves, in comparison with

plate-like structures [24]. The main purpose of this study is therefore to quantify the relation between the nonlinear parameter and crack length in pipe structures using numerical and experimental analyses.

In this paper appropriate mode selection for the generation of second harmonic in pipe structures is first introduced to provide a basis for the subsequent numerical and experimental studies. Numerical modelling and results are then presented, followed by a fatigue test as experimental verification for comparison with the simulation results and for investigating the nonlinearity induced by a fatigue crack. The comparisons between simulation and experiment results are conducted and the possible reasons are justified by a further simulation study. Finally, the conclusions of the study are drawn.

2. Selection of excitation wave

For appropriate wave mode selection for the second harmonic generation, a dispersion curve of an aluminium pipe (30 mm outer diameter and 4 mm wall thickness) was plotted by DISPERSE, as in Figure 1. Longitudinal wave mode L(0, 2) was selected as the fundamental wave due to its fastest group velocity and non-dispersive properties within a wide range of frequency. The excitation frequency was 300 kHz, such that the L(0, 2) mode would convert to the L(0, 3) mode at the double frequency 600 kHz. Since the velocities of those two wave modes were different, the cumulative effect caused by material nonlinearity could be minimised and the second harmonic generated by a fatigue crack could be highlighted. It could be noticed from the dispersion curve that a group of flexural wave modes F(n, 2) had group velocities similar to that of the longitudinal wave mode L(0, 2), especially when $n \leq 2$. Therefore, when a single surface-bonded actuator was applied, it would generate multiple modes at the excitation frequency.

In this study, a notation for the classification of wave modes from Rose [25] was adopted, where L(n, m) stands for a longitudinal mode group consisting of axisymmetric modes L(0, m) and non-axisymmetric modes F(n, m), where *n* is defined as the circumferential order of a mode and *m* denotes the group order. Therefore, the waves at fundamental frequency for the pipe under investigation were generated as a group of wave modes L(n, 2) composed of a longitudinal mode L(0, 2) and flexural modes F(n, 2) (n=1,2,3…) which would then be converted by a fatigue crack to L(n, 3) modes at the second harmonic, consisting of L(0, 3) and F(n, 3) modes.

3. Methods

3.1 3D Finite element model

A 3D model in Abaqus/Explicit was utilised to simulate the wave propagation, material nonlinearity and the CAN in a pipe. The pipe model dimensions were wall thickness 4 mm, outer diameter 30 mm and length 1 m. For fatigue crack initiation, an 8 mm long 2 mm wide through-thickness notch was modelled by removing corresponding elements from the pipe. A 6-cycle Hann-window tone burst signal with the central frequency at 300 kHz was excited and was applied as point loads at four edges of the actuator in the pipe axis direction. A group of L(n, 2), including the longitudinal mode L(0, 2) and flexural modes F(n, 2) at the excited frequency, was generated due to the actuation of one transducer. Two receiving points were set separately at two sides of the notch so as to receive both wave transmission and reflection. Details of the locations of the transducers and monitoring points are presented in Figure 2.

The element type in this model was selected as 3D eight-node brick elements (C3D8R) and with element size of 1 mm, which resulted in about 18 elements per wavelength of the fundamental wave mode L(0, 2) and 12 elements per wavelength of the second harmonic wave mode L(0, 3). On the basis of the equation $\Delta t \leq L_{max}/c_g$ [26], a time step 5e-8 s was selected

for accuracy and stability of the model, where L_{max} is the maximum element size and c_g is the fastest group velocity among all wave modes propagating in the model.

To simulate the "breathing" crack, built-in definition known as seam crack in Abaqus was set on the surfaces of the crack and then a surface-to-surface contact interaction was assigned on the crack to achieve breathing behaviour subjected to propagating waves [8], as illustrated in Figure 3(a), where the through-thickness fatigue crack exists at both tips of the notch. In Figure 3(b), it can be recognised that the compressional part of the wave closes the crack and as a result the stress can pass through, whereas in Figure 3(c), the tensional part of the wave opens the crack and the stress is blocked by the crack. In order to analyse the relation between the nonlinear parameter and the crack length, the crack was increased from 1 mm to 14 mm in length at each tip with an increment of 0.5 mm, 1 mm or 2 mm in the circumferential direction till it reaches about half the circumference of the pipe. Since the material itself contains nonlinearity homogenously in the pipe in the experiment, apart from CAN from a breathing crack, material nonlinearity was also included in the model via setting material properties with third order elastic constants [17], which were merged into the model through a user subroutine file [8]. The basic material properties as well as the third order elastic constants are listed in Table 1.

3.2 Experimental procedure

An aluminium pipe with the same configurations as in the simulation model was utilised in experiment. Here, 5 mm × 10 mm rectangular and 5 mm × 5 mm square surface-bonded piezoelectric transducers were used as actuator and receivers in the experiment, with the same arrangements as in the simulation. A system for generating and collecting signals was deployed in the experimental testing, which included a Ritec RAM-5000 SNAP and an Agilent digital

oscilloscope. A high-power low-pass filter was connected to the system so as to filter out harmonics higher than the fundamental frequency from other sources.

With the same excitation signal as in simulation, the reflection and transmission wave signals were recorded before the fatigue test as benchmark signals. The pipe was then subjected to the three-point bending on a fatigue machine with a cyclic compressional load in the middle. The applied load ranged from 0.2 kN to 2 kN, with the equivalent highest stress on the cross section at about 50% of the yield stress of the pipe, and the loading frequency was at 2 Hz. During fatigue testing, the signals were continuously collected every 2000 cycles until 22000 cycles, after which the interval for signal collection was changed to 4000 cycles. Fatigue testing was stopped at 42000 cycles when the nonlinearity in the received signals dropped to noise level. Signals were recorded after 1024 times average with a 200 MHz sampling frequency. It should be noted that during each moment of signal collection the fatigue machine was unloaded to avoid any adverse effect of the applied loads on the opening and closure behaviour of the fatigue crack.

4. Results

4.1 Transmission and reflection characteristics

4.1.1 Simulation results

A typical transmitted signal before introduction of the simulated crack is in Figure 4. It is observed that more than one wave packet arrives in the interest of time period because of the single actuator excitation. The first wave arrives at 83 μs, which is in accordance with the group velocity of the L(0, 2) mode from the dispersion curve while the subsequent waves are flexural modes F(n, 2). To extract the waves at double frequency, after collecting all the signals, the input signal was flipped 180° (i.e. out-of-phase) and then was applied to the specimen again at the same location, followed by same signal collection procedures. These two received signals

were added together to reduce the contribution of the fundamental wave component and to highlight the second harmonic [27]. Subsequently, each of the combined signals was processed with a short-time Fourier transform (STFT) to extract the slices at double frequency which were then transformed back to the time domain by the inverse fast Fourier transform [8]. Meanwhile, to obtain signals at the fundamental frequency, the received signals before combined with their out-of-phase counterparts were directly processed with STFT and the slices at fundamental frequency were also extracted. With such a procedure, the time domain signals of interest at the fundamental and double frequencies were obtained for further analysis.

Transmitted signals after processing procedure as above are demonstrated in Figure 5. In comparison with the benchmark signal where only material nonlinearity was introduced, the cases with 1 mm and 2 mm seam cracks at the fundamental frequency show minor differences in Figure 5(a) and (b), whereas the second harmonic wave arrives at the time later than the fundamental one, mainly due to the reason that the group velocity of L(0, 3) induced by the microcrack at double frequency is slower than that of L(0, 2) at fundamental frequency. For both 1 mm and 2 mm seam crack cases, multiple waves are induced at double frequency as in Figure 5(c) before the arrival of L(0, 1), which is a group of wave modes L(n, 3), including the fastest L(0, 3) mode and F(n, 3) modes. It can be calculated that the average amplitude level of the second harmonic wave for the 2 mm crack case is about 1.4% of the wave at the fundamental frequency, slightly greater than that of the 1 mm crack case, which is approximately 1.3% of the fundamental wave. However both are still much higher than that caused by material nonlinearity in benchmark as shown in Figure 5(d). Similarly, nonlinearity induced by micorcrack was also observed in the reflected signals at double frequency, as in Figure 6. The average amplitude of the second harmonic wave of the 2 mm crack case is about 2.3% of the wave at the fundamental frequency and is greater than that of the 1 mm crack case,

and both of them are much higher than that in the benchmark where material nonlinearity only is considered.

4.1.2 Experimental results

The transmitted signal before fatigue test is shown in Figure 7. The first wave packet arrives almost at the same time as that in simulation, and multiple wave packets known as L(n, 2) modes also appear before the arrival time of L(0, 1) mode at 126 μs, similar to the observation in simulation results. The waveform of the signal received experimentally was somewhat different from the simulation results, which however is still acceptable in the consideration of inevitable difference between experiment and simulation such as the actual performance of the transducer to efficiently generate different wave modes in experiment.

As compared in Figure 8(a) for the benchmark signal before the fatigue test and the signals at 12000 and 22000 fatigue cycles, signals for the damage cases show no obvious difference from the benchmark at fundamental frequency. In the comparison between those two damage cases at double frequency in Figure 8(b), the average amplitude level of the second harmonic wave after 22000 cycles is more than 2% of the wave at the fundamental frequency, which is obviously higher than the case after 12000 cycles; more importantly, both damage cases show greater nonlinearity than that in the benchmark. Furthermore, it can be seen in Figure 8(b) that the second harmonic wave from both damage cases arrives later than the benchmark signal and more than one wave packet is generated, which was similar with the simulation results.

On the other hand, the average amplitude of the second harmonic wave of the benchmark, which is about 0.8% of that at fundamental frequency, is much higher than that in simulation. This difference can be attributed to unavoidable nonlinearities from equipment and environment, together with the material nonlinearity of the actual pipe which was not ideally homogeneous. The reflected signals also show similar results in Figure 9, whereas the

multimode second harmonic waves are not as obvious as in the transmitted signals. This is because of the shorter distance between the sensor for reflection and the fatigue crack where the multiple wave modes with close velocities are not completely separated.

4.2 Nonlinear index with growth of fatigue crack

4.2.1 Nonlinear parameter

From the analysis of signals received in simulation and experiment, it could be observed that the nonlinearity changed with the crack length and fatigue cycle respectively. Generally, a relative nonlinear parameter $\beta'=A_2/A_1^2$ is used to assess the nonlinearity in a system, where A_1 and A_2 are the amplitudes of fundamental wave and second harmonic wave in the time domain [28, 29] or frequency domain [30, 31]. However, due to the multiple wave mode generation at fundamental and double frequencies and the nonlinearity is mainly from the crack breathing behaviour, the conventional relative nonlinear parameter is not suitable to evaluate the CAN in pipe structures. A proper parameter in the time domain was proposed in a previous study [24] to include all the wave packets induced by damage in order to evaluate quantitatively the nonlinearity induced by the breathing crack in the pipe. In this study, the nonlinear parameter for both transmission and reflection was defined as the integral of the amplitude profile of L(n, 3) before the arrival time of L(0, 1) at double frequency divided by the integral of the amplitude profile of L(n, 2) before the arrival time of L(0, 1) at fundamental frequency. Such a nonlinear index was calculated for all the damage cases in experiment and simulation and was used as a measurement of the nonlinearity in the pipe so as to quantify the severity of the fatigue crack.

4.2.2 Nonlinear indices from simulation

As observed in Figure 10, for both transmitted and reflected signals the nonlinear index increases monotonously with crack length until the crack length reaches around 6 mm at each

notch tip where the index reaches a relatively constant value and then it begins to drop to approximately half of the maximum value. The nonlinear index close to zero at 0 mm crack length is the benchmark signal which contains material nonlinearity only, indicating that the material nonlinearity can be disregarded when compared with the damage cases. It is interesting that the total crack length for both tips (12 mm) when nonlinearity reaches the maximum is close to the wavelength of the second harmonic wave, which is around 13 mm. It was understood that the increase in nonlinearity was mainly caused by the increase in the portion of the crack which could be completely closed and opened by the incident wave. However, when the crack length became fairly long, e.g. longer than 6 mm in this study, since the closure of the far edge of the crack depends on the waves that detour to it, vibration of the far edge of the crack was minimised because the incident wave was incapable of detouring to the middle part of the crack and only the edge of the crack close to the actuator kept vibration. In such cases, part of the crack had evolved into an open crack, where only the tip of the seam crack is still assumed to show breathing behaviour which contributed to the nonlinearity. To confirm this assumption, signals at fundamental frequency were extracted for different crack cases as in Figure 11. It can be seen that for models with 2 mm and 6 mm crack, the amplitudes of fundamental wave were similar to the benchmark. However, the reflected and transmitted signals start to change for the case of 8 mm crack, indicating the change of the close crack to the open one.

It is well-known that the second harmonic amplitude would have a quadratic increase with input voltage level due to material nonlinearity which can be described by a relative nonlinear parameter $\beta' = A_2/A_1^2$ [32]. To further figure out the influence of input energy on the CAN, the numerical model was re-simulated with the input load ten times higher than that in the original model. It is confirmed that the second harmonic amplitude due to the CAN shows linear rather

quadratic increase with input voltage. Therefore, the trend of nonlinear index in Figure 10 will not change with variation in input signals.

Two FE models based on the original one were further developed to verify the reason of nonlinearity decrease in Figure 10. The curves in Figure 10 indicate that the nonlinear indices for 3 mm and 10 mm long cracks (at each tip of the notch) were similar. On the basis of the aforementioned assumption, the middle part (7 mm) of the 10 mm seam crack would become open when the waves passed through. Therefore, the length of the notch was extended in the numerical model from the original 8 mm to 22 mm in the middle, where 14 mm represents the middle part of two 10 mm seam cracks (7 mm at each tip) that has become open. Thus only 3 mm seam cracks at the two tips of the new notch were created, as shown in Figure 12. In the updated model in Figure 12(b), the pipe dimension, material properties and mesh setting were all the same as in original model, as was the simulation method of the breathing crack and material nonlinearity. Similarly, for the 4 mm and 8 mm crack cases which also show similar nonlinearity in Figure 10, the same procedure was conducted for the second updated model, where the length of the notch was extended from the original 8 mm to 16 mm in the middle.

The resultant nonlinear index from the reflected signals for first updated model (for the 3 mm and 10 mm long crack cases) is 0.0228 (shown as a red dot in Figure 10), which is comparable to the nonlinear index from the 3 mm crack length case at 0.0235 and the 10 mm crack length at 0.0224. Similar results are also observed from the transmitted signals (shown as a red square in Figure 10), where the value from the updated model is 0.0182, between 0.0171 (for 3 mm crack length) and 0.0202 (for 10 mm crack length). Similarly, nonlinearity indices 0.0371 and 0.0279 for the reflected and transmitted signals were obtained in the second updated model (for the 4 mm and 8 mm long crack cases), respectively (shown as a green dot and a green square in Figure 10, respectively), which are also close to the values from the model with 4 mm close crack. These results confirm the assumption that the decrease of nonlinearity in the simulation

model was due to the disappearance of breathing behaviour in the middle part of the crack, which becomes an open crack to the incident guided waves.

4.2.3 Experimental result

The nonlinear indices were also calculated for all received signals in experiment under different fatigue cycles as shown in Figure 13, which is curve-fitted using a fifth order polynomial function. It can be seen that the nonlinear index increases gradually with the fatigue cycle until about 26000 cycles and then decreases to the same level as in the benchmark. It is understood that the initiation of fatigue crack includes the accumulation of material dislocation around the notch tips and the formation of microcracks, which contribute to the increase in wave nonlinearity. Then the crack developed from a microcrack to an open crack, no longer generating the CAN. It should be mentioned that at the end of the fatigue test, the crack length observed in the experiment was about 1 mm, which was only at the beginning stage of the simulation model. The increasing part of nonlinear index with crack length from simulation and experiment is both because of the increasing length of the crack that contributes to the nonlinearity. However, the nonlinear index in the experiment began to drop at an early stage, indicating that different to numerical simulation, the breathing behaviour in practice existed only at the early stage of a fatigue crack, which would become an open crack immediately upon growing to a macro scale.

To confirm this assumption, some typical transmitted and reflected signals at fundamental frequency are plotted in Figure 14, including signals at benchmark, 12000, 22000, 34000 and 42000 fatigue cycles. As evident in the Figure, for the transmitted L(0, 2) and F(n, 2) modes, the wave amplitudes are close to each other until 22000 fatigue cycles and the amplitudes at 34000 and 42000 fatigue cycles are obvious smaller than the other cases. Also, before 22000 fatigue cycles, there is no noticeable difference in the reflected L(0, 2) from the notch. However, the reflected fundamental wave L(0, 2) clearly increases at 34000 and 42000 cycles, revealing

that the crack evolves from micro to macro one and even the fundamental wave may be capable of detecting its existence.

5. Conclusions

The relation between cylindrical nonlinear waves and a fatigue crack in an aluminium pipe was comprehensively investigated in this study with the consideration of the existence of multiple wave modes in the pipe structure. Both numerical and experimental studies were carried out considering material nonlinearity and CAN while the differences between experimental and simulation results were discussed. In the simulation model, the seam crack length was continuously increased to simulate growth of a fatigue crack. For the experimental testing while a fatigue machine was used for fatigue crack generation and piezoelectric transducers were adopted for the acquisition of wave nonlinearity.

From the numerical simulation, it was found that the nonlinear index first increased monotonously with crack length because of the increasing length of the breathing crack but began to decrease at a specific crack length which is close to the wavelength of the second harmonic wave. After that the crack was evolved from micro to macro scale as an open crack, where the signal changes in the fundamental frequency start to be dominant with the further growth of the crack. However, in the experiment the nonlinear index starts to drop at early stage, indicating in practice the CAN only exists at initial stage of fatigue crack. The results from both studies show that the nonlinear index can quantify the nonlinearity in a pipe structure caused by crack and it can detect the initial stage of a fatigue crack within 1 mm in practice, providing higher sensitivity than linear guided waves for microcrack detection.

Acknowledgement

Zhongqing Su is grateful to the Hong Kong Research Grants Council for support via General Research Funds (No. 15201416 and 15212417). This work was also partially supported by the National Natural Science Foundation of China (No. 51635008).

References

[1] R. Guan, Y. Lu, W. Duan, and X. Wang, "Guided waves for damage identification in pipeline structures: A review," *Structural Control and Health Monitoring,* vol. 24, pp. e2007-e2007-17, 2017.

[2] D. N. Alleyne, M. J. S. Lowe, and P. Cawley, "The reflection of guided waves from circumferential notches in pipes," *Applied Mechanics,* vol. 65, pp. 635-641, 1998.

[3] A. Demma, P. Cawley, M. Lowe, A. G. Roosenbrand, and B. Pavlakovic, "The reflection of guided waves from notches in pipes: a guide for interpreting corrosion measurements," *NDT & E International,* vol. 37, pp. 167-180, 2004.

[4] S. Heinlein, P. Cawley, and T. K. Vogt, "Reflection of torsional T(0,1) guided waves from defects in pipe bends," *NDT & E International,* vol. 93, pp. 57-63, 2018.

[5] M. Kharrat, M. N. Ichchou, O. Bareille, and W. Zhou, "Pipeline inspection using a torsional guided-waves inspection system. Part 1: Defect identification," *International Journal of Applied Mechanics,* vol. 06, pp. 1450034-1450034-24, 2014.

[6] D. Broda, W. J. Staszewski, A. Martowicz, T. Uhl, and V. Silberschmidt, "Modelling of nonlinear crack–wave interactions for damage detection based on ultrasound—a review," *Journal of Sound and Vibration,* vol. 333, pp. 1097-1118, 2014.

[7] X. Wan, Q. Zhang, G. Xu, and P. W. Tse, "Numerical simulation of nonlinear Lamb waves used in a thin plate for detecting buried micro-cracks," *Sensors,* vol. 14, pp. 8528-8546, 2014.

[8] M. Hong, Z. Su, Q. Wang, L. Cheng, and X. Qing, "Modeling nonlinearities of ultrasonic waves for fatigue damage characterization: Theory, simulation, and experimental validation," *Ultrasonics,* vol. 54, pp. 770-778, 2014.

[9] P. Blanloeuil, L. R. F. Rose, J. A. Guinto, M. Veidt, and C. H. Wang, "Closed crack imaging using time reversal method based on fundamental and second harmonic scattering," *Wave Motion,* vol. 66, pp. 156-176, 2016.

[10] Y. Shen and C. E. Cesnik, "Modeling of nonlinear interactions between guided waves and fatigue cracks using local interaction simulation approach," *Ultrasonics,* vol. 74, pp. 106-123, 2017.

[11] M. J. Leamy, T. B. Autrusson, W. J. Staszewski, T. Uhl, and P. Packo, "Local computational strategies for predicting wave propagation in nonlinear media," in *SPIE Smart Structures and Materials + Nondestructive Evaluation and Health Monitoring,* 2014, p. 15.

[12] M. Ryles, F. H. Ngau, I. Mcdonald, and W. J. Staszewski, "Comparative study of nonlinear acoustic and Lamb wave techniques for fatigue crack detection in metallic

structures," *Fatigue & Fracture of Engineering Materials & Structures,* vol. 31, pp. 674-683, 2008.

[13] C. Pruell, J.-Y. Kim, J. Qu, and L. J. Jacobs, "Evaluation of fatigue damage using nonlinear guided waves," *Smart Materials and Structures,* vol. 18, pp. 035003-035003-7, 2009.

[14] R. Soleimanpour, C.-T. Ng, and C. H. Wang, "Higher harmonic generation of guided waves at delaminations in laminated composite beams," *Structural Health Monitoring,* vol. 16, pp. 400-417, 2017.

[15] W. Li, Y. Cho, and J. D. Achenbach, "Detection of thermal fatigue in composites by second harmonic Lamb waves," *Smart Materials and Structures,* vol. 21, p. 085019, 2012.

[16] C. Mattei and P. Marty, "Imaging of fatigue damage in CFRP composite laminates using nonlinear harmonic generation," in *AIP Conference Proceedings,* 2003, pp. 989-995.

[17] W. J. De Lima and M. F. Hamilton, "Finite amplitude waves in isotropic elastic waveguides with arbitrary constant cross-sectional area," *Wave Motion,* vol. 41, pp. 1-11, 2005.

[18] Y. Liu, C. J. Lissenden, and J. L. Rose, "Higher order interaction of elastic waves in weakly nonlinear hollow circular cylinders. I. Analytical foundation," *Journal of Applied Physics,* vol. 115, pp. 214901-214901-11, 2014.

[19] Y. Liu, E. Khajeh, C. J. Lissenden, and J. L. Rose, "Higher order interaction of elastic waves in weakly nonlinear hollow circular cylinders. II. Physical interpretation and numerical results," *Journal of Applied Physics,* vol. 115, pp. 214902-214902-10, 2014.

[20] Y. Liu, E. Khajeh, C. J. Lissenden, and J. L. Rose, "Interaction of torsional and longitudinal guided waves in weakly nonlinear circular cylinders," *The Journal of the Acoustical Society of America,* vol. 133, pp. 2541-2553, 2013.

[21] W. Li and Y. Cho, "Thermal fatigue damage assessment in an isotropic pipe using nonlinear ultrasonic guided waves," *Experimental Mechanics,* vol. 54, pp. 1309-1318, 2014.

[22] Y. Wang and J. D. Achenbach, "The effect of cubic material nonlinearity on the propagation of torsional wave modes in a pipe," *The Journal of the Acoustical Society of America,* vol. 140, pp. 3874-3883, 2016.

[23] M. Deng, G. Gao, Y. Xiang, and M. Li, "Assessment of accumulated damage in circular tubes using nonlinear circumferential guided wave approach: A feasibility study," *Ultrasonics,* vol. 75, pp. 209-215, 2017.

[24] R. Guan, Y. Lu, K. Wang, and Z. Su, "Fatigue crack detection in pipes with multiple mode nonlinear guided waves," *Structural Health Monitoring,* vol. 0, p. 1475921718791134, 2018.

[25] J. L. Rose, *Ultrasonic guided waves in solid media*. New York: Cambridge University Press, 2014.

[26] O. Diligent, T. Grahn, A. Boström, P. Cawley, and M. J. S. Lowe, "The low-frequency reflection and scattering of the S0 Lamb mode from a circular through-thickness hole in a plate: Finite Element, analytical and experimental studies," *The Journal of the Acoustical Society of America,* vol. 112, pp. 2589-2601, 2002.

[27] J.-Y. Kim, L. J. Jacobs, J. Qu, and J. W. Littles, "Experimental characterization of fatigue damage in a nickel-base superalloy using nonlinear ultrasonic waves," *The Journal of the Acoustical Society of America,* vol. 120, pp. 1266-1273, 2006.

[28] C. Pruell, J.-Y. Kim, J. Qu, and J. J. Laurence, "Evaluation of fatigue damage using nonlinear guided waves," *Smart Materials and Structures,* vol. 18, p. 035003, 2009.

[29] P. Zuo, Y. Zhou, and F. Zheng, "Numerical studies of nonlinear ultrasonic guided waves in uniform waveguides with arbitrary cross sections," *AIP Advances,* vol. 6, p. 075207, 2016.

[30] Y. Yang, C.-T. Ng, A. Kotousov, H. Sohn, and H. J. Lim, "Second harmonic generation at fatigue cracks by low-frequency Lamb waves: Experimental and numerical studies," *Mechanical Systems and Signal Processing,* vol. 99, pp. 760-773, 2018.

[31] W. Li and Y. Cho, "Combination of nonlinear ultrasonics and guided wave tomography for imaging the micro-defects," *Ultrasonics,* vol. 65, pp. 87-95, 2016.

[32] J. Herrmann, J.-Y. Kim, L. J. Jacobs, J. Qu, J. W. Littles, and M. F. Savage, "Assessment of material damage in a nickel-base superalloy using nonlinear Rayleigh surface waves," *Journal of Applied Physics,* vol. 99, p. 124913, 2006.

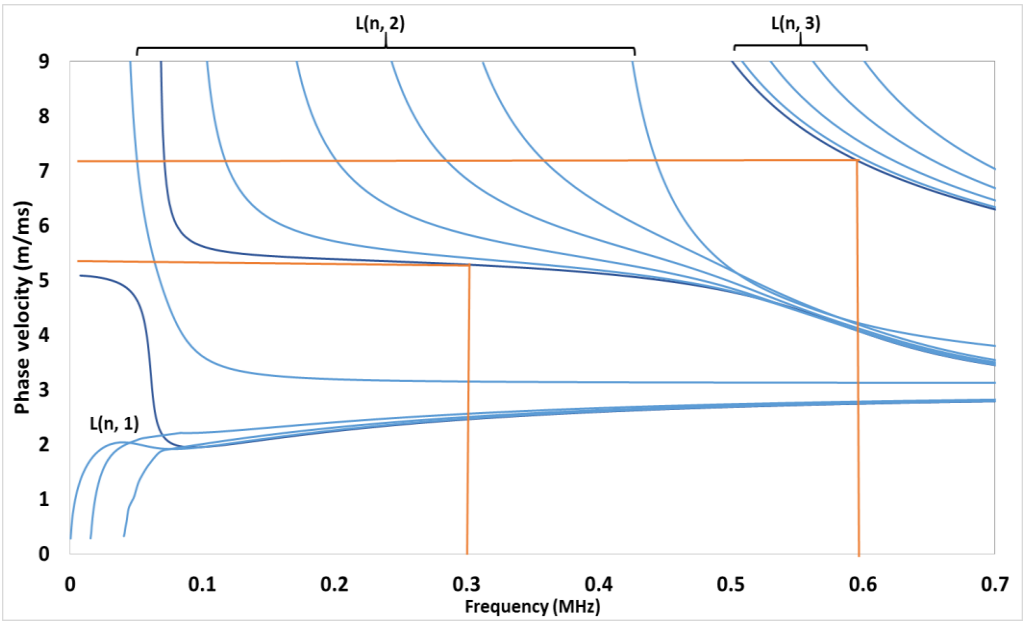

(a)

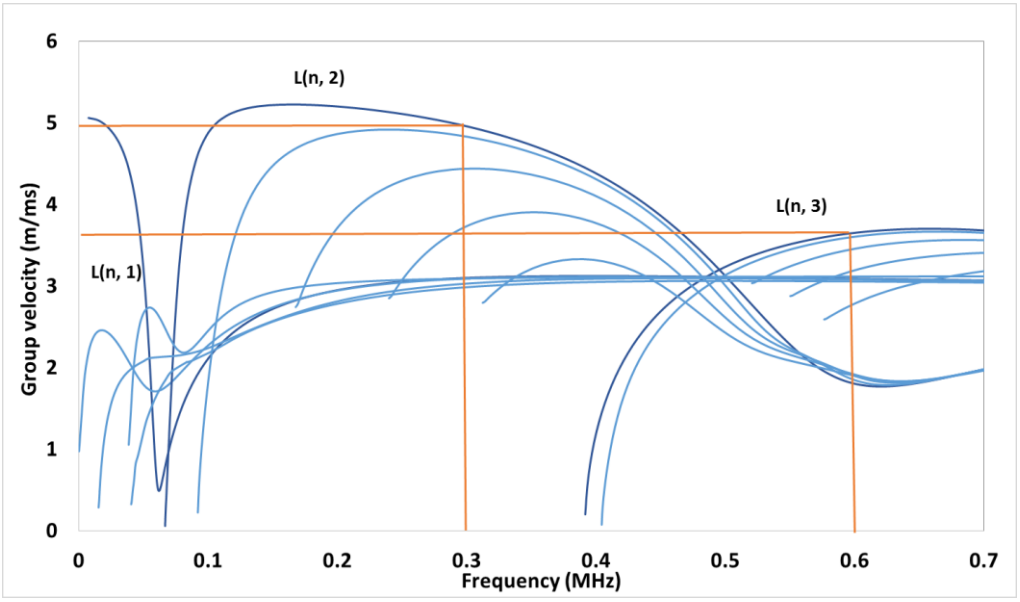

(b)

Figure 1 Dispersion curve of aluminium pipe with 20 mm diameter and 4 mm wall thickness. (a) Phase velocity; (b) Group velocity

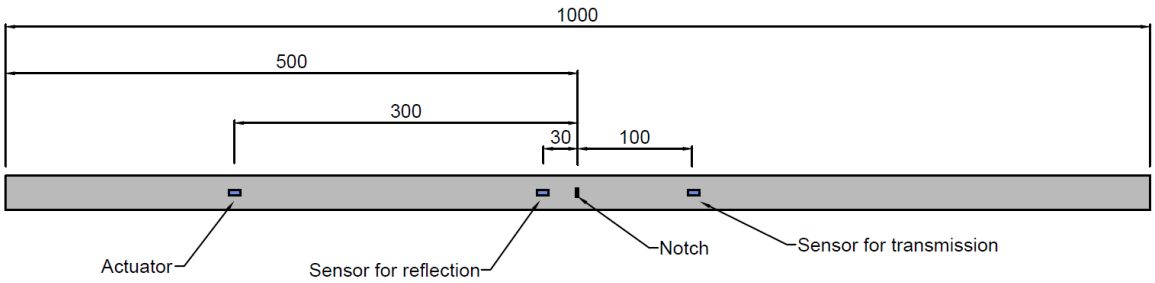

Figure 2 Arrangement of actuator and sensors (unit: mm)

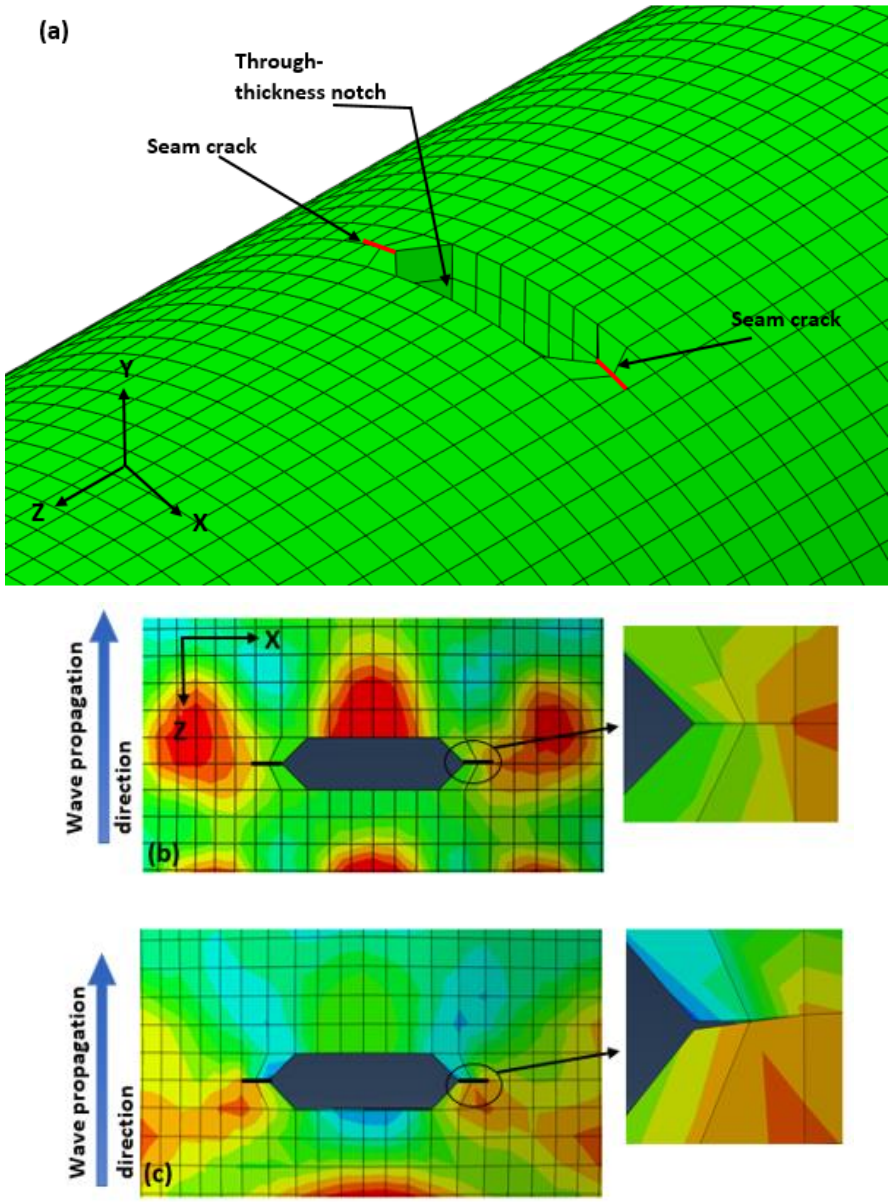

Figure 3 Nonlinear wave simulation in finite element analysis (a) seam crack in simulation model; (b) waves pass through the seam crack when it closes; (c) waves are blocked by the seam crack when it opens

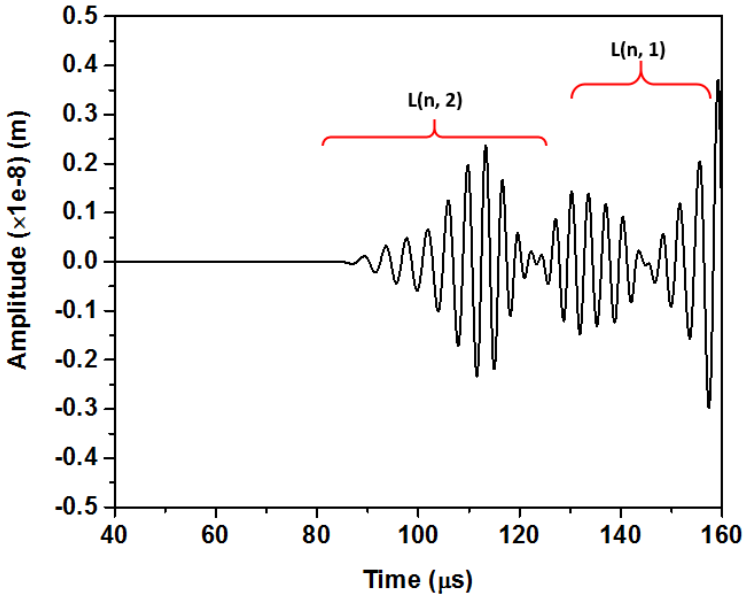

Figure 4 Typical transmitted signal from simulation

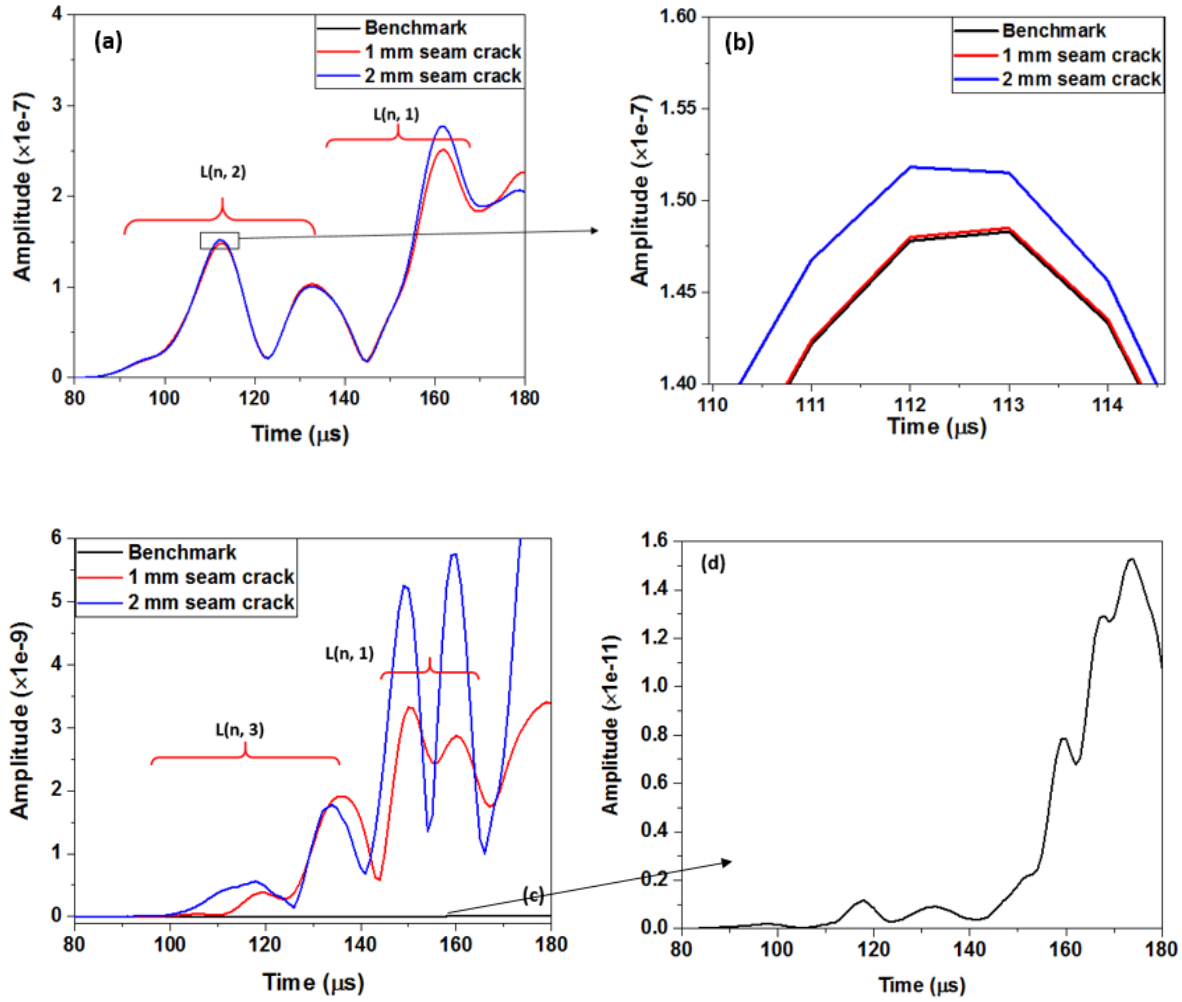

Figure 5 Transmitted signal from simulation with CAN after STFT compared with benchmark signals (a) at fundamental frequency; (b) signals at fundamental frequency after zoomed in; (c) signals at double frequency and (d) benchmark signal at double frequency.

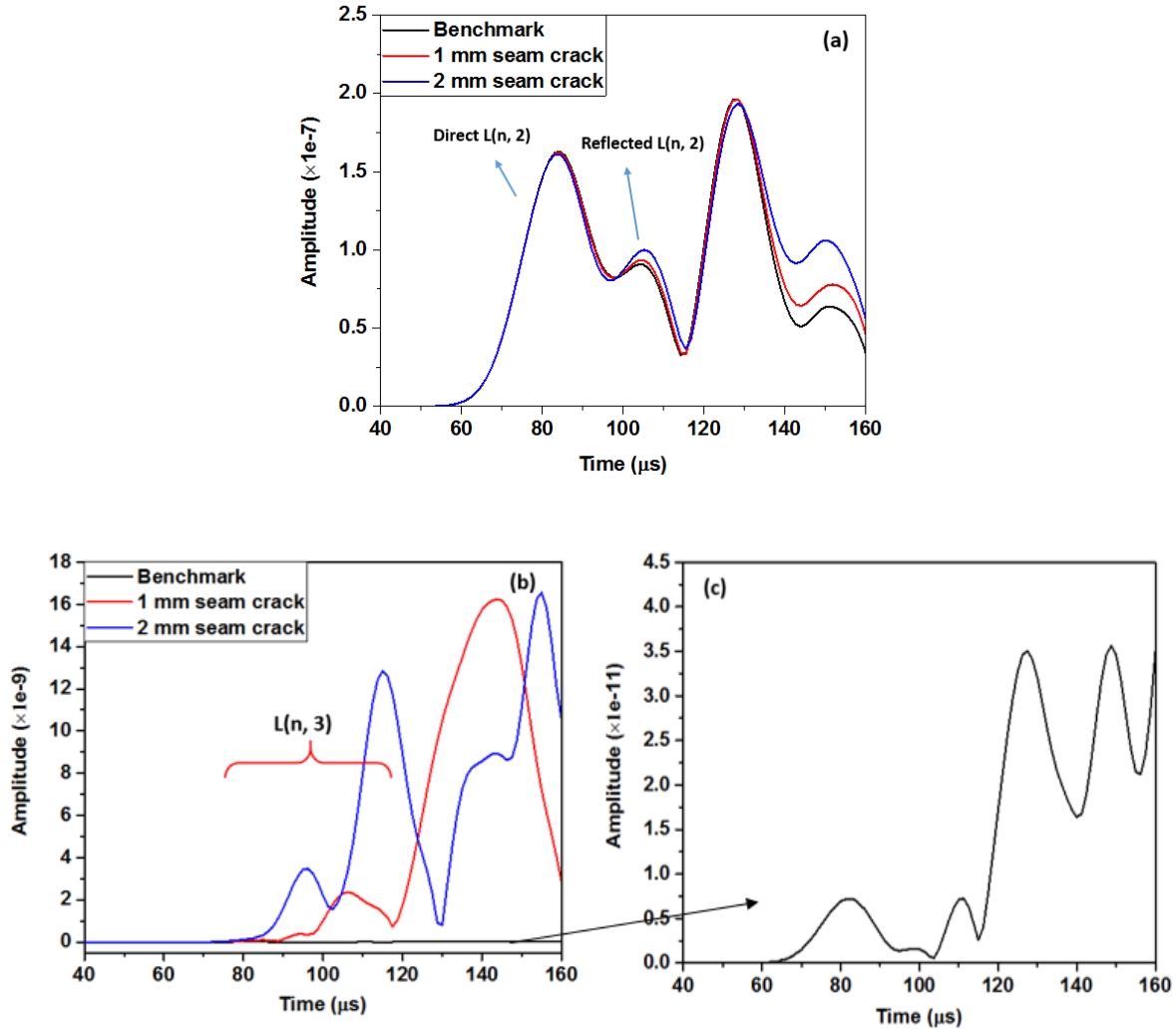

Figure 6 Reflected signal from simulation with CAN after STFT compared with benchmark signals (a) at fundamental frequency; (b) at double frequency and (c) benchmark signal at double frequency.

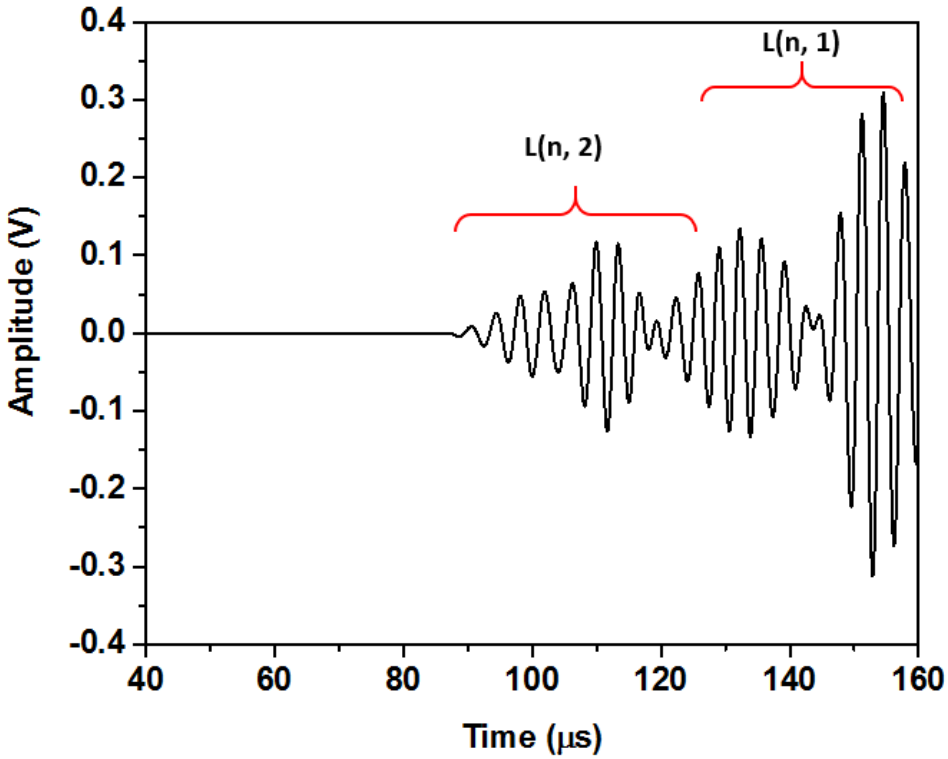

Figure 7 Transmitted signal from experiment

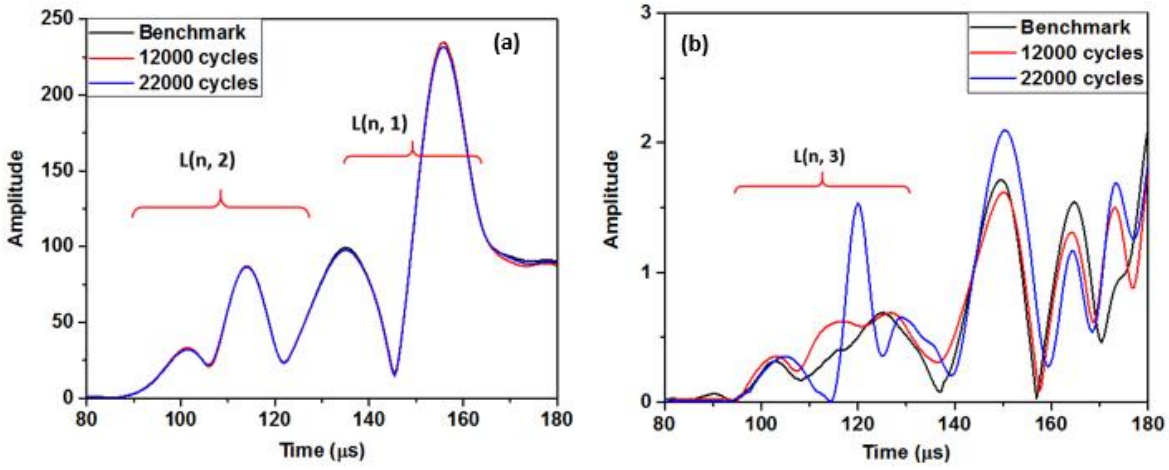

Figure 8 Transmitted signal from experiment at different fatigue cycles compared with benchmark signal (a) at fundamental frequency; (b) at double frequency

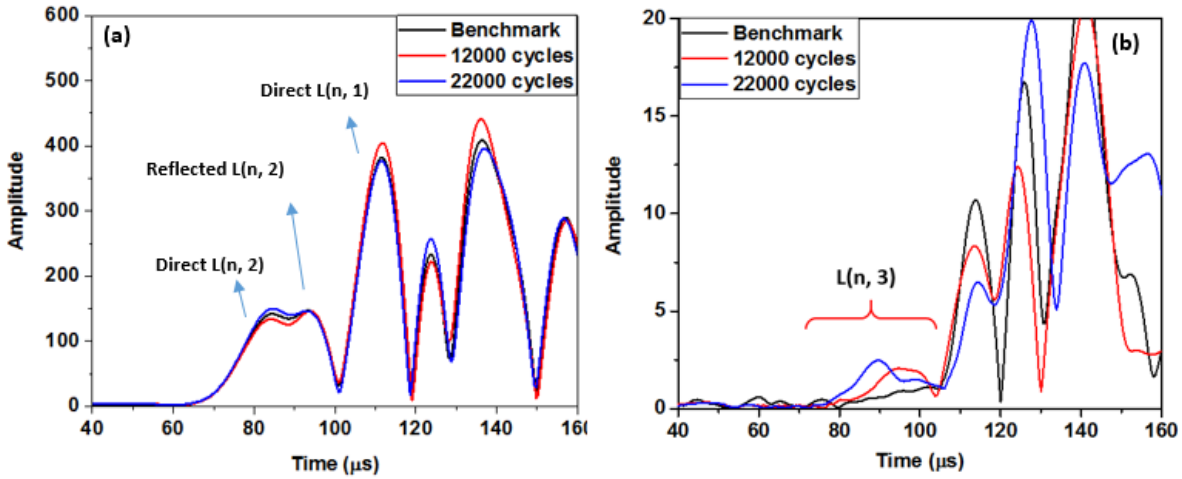

Figure 9 Reflected signal from experiment at different fatigue cycles compared with benchmark signal (a) at fundamental frequency; (b) at double frequency

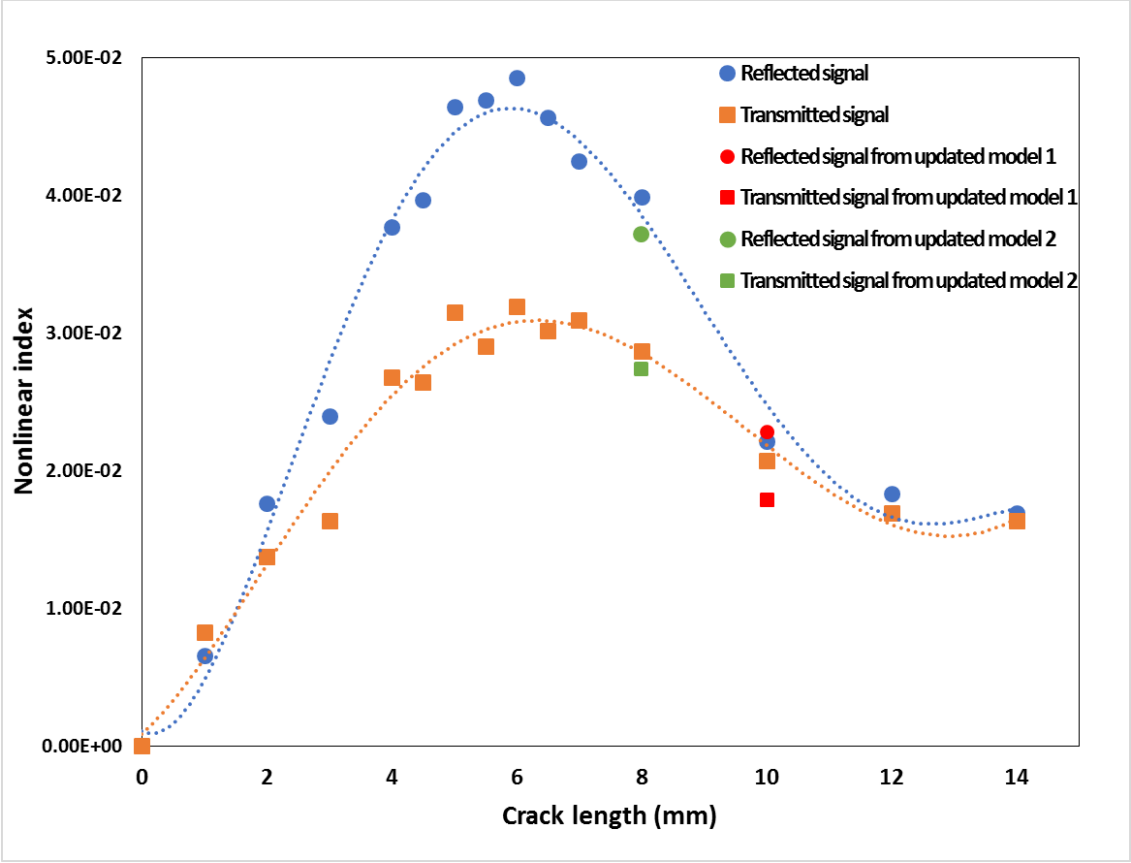

Figure 10 Nonlinear index vs crack length at each tip of notch in simulation

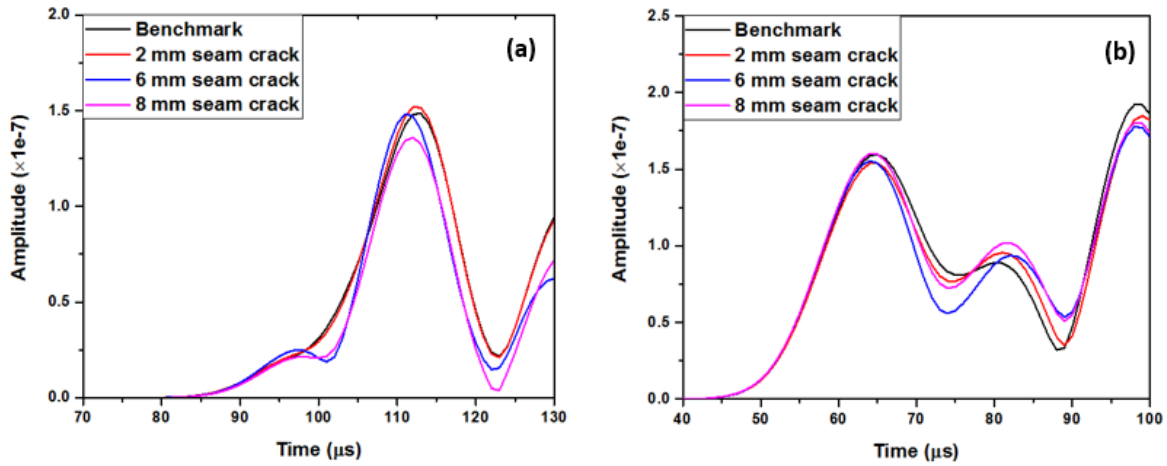

Figure 11 (a) Transmitted and (b) reflected signals at fundamental frequency from simulation model for benchmark, 2 mm, 6 mm and 8 mm seam crack cases

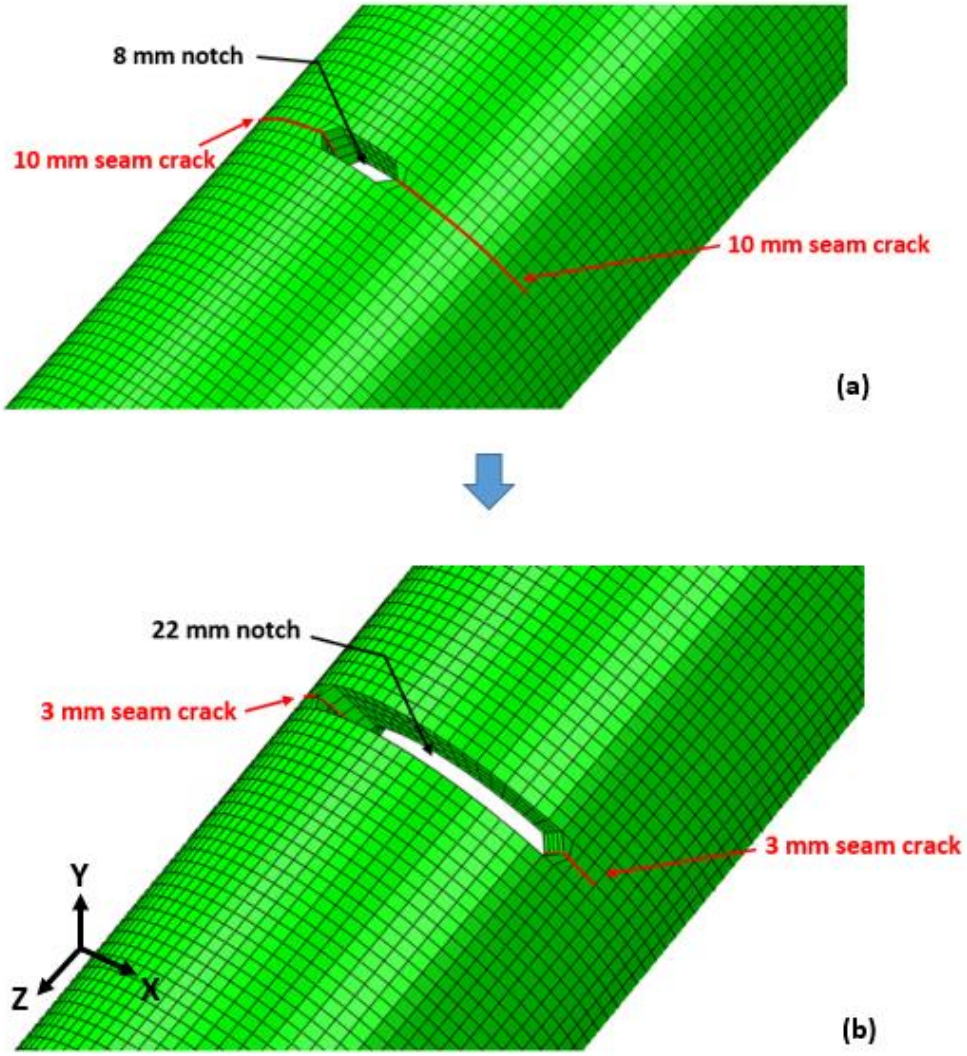

Figure 12 (a) Original model; (b) updated model with notch extended in the middle

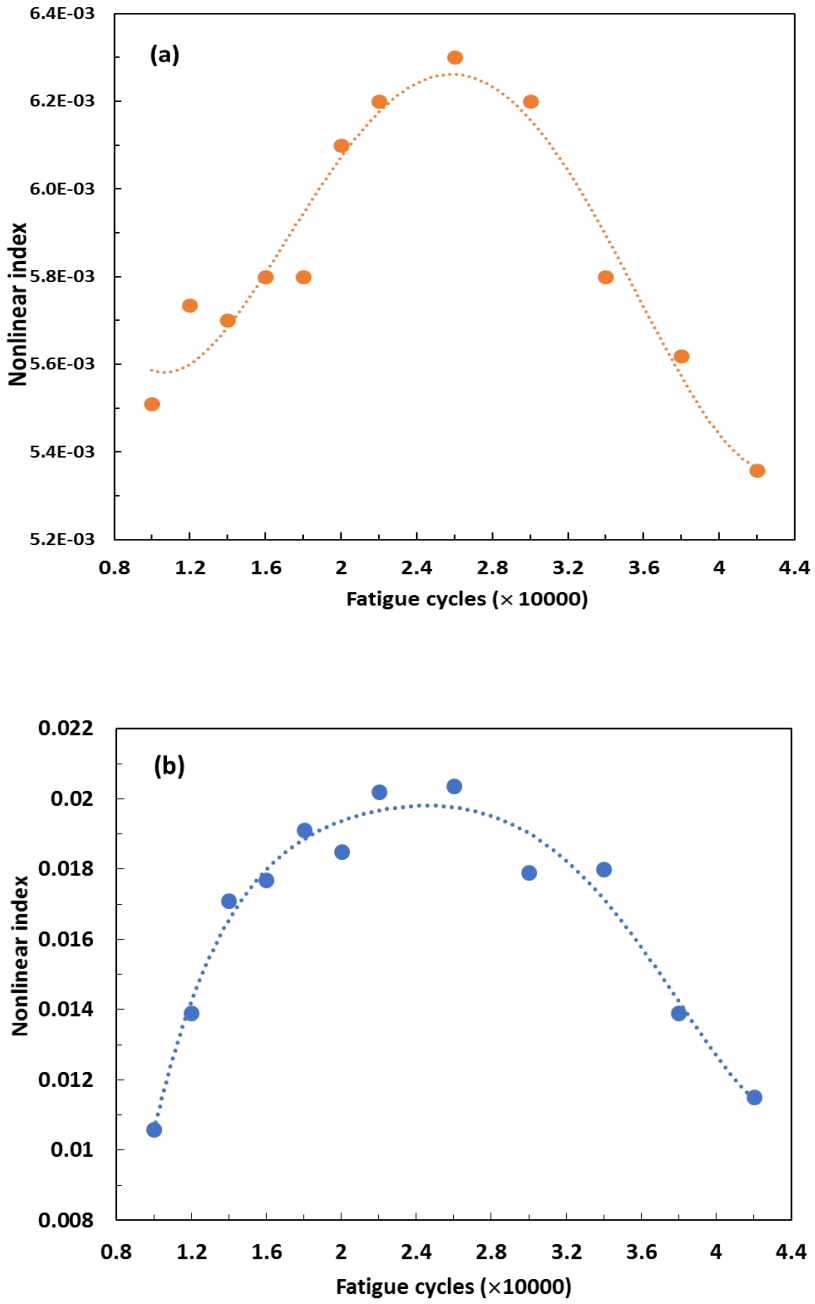

Figure 13 Nonlinear index vs fatigue cycle from experimental testing for (a) transmitted signals; (b) reflected signals

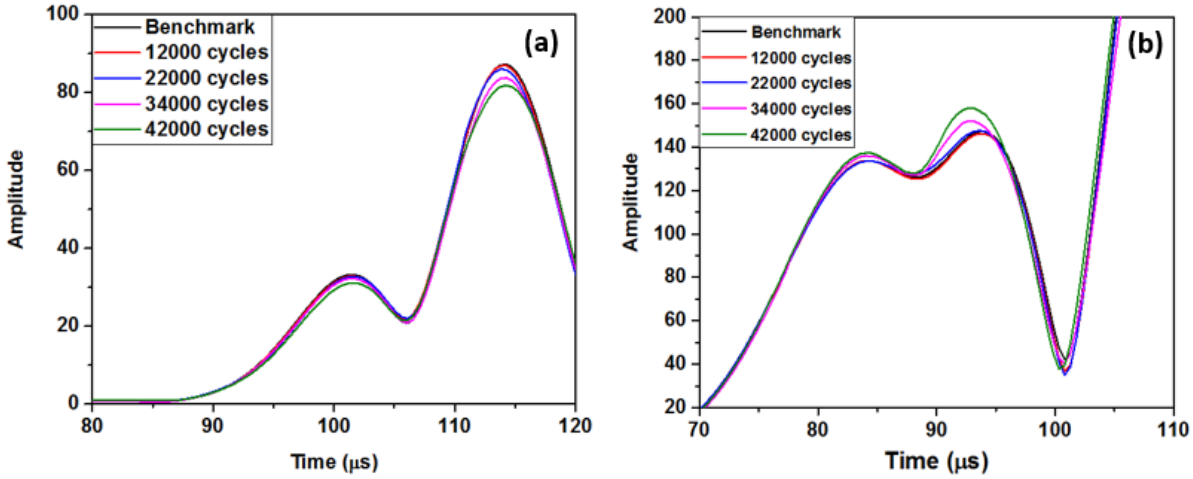

Figure 14 (a) Transmitted signal and (b) reflected signals under different fatigue cycles at fundamental frequency

Table 1 Material properties input for simulation model

Material properties		
Density (kg/m^3)		2700
Young's modulus (GPa)		68.9
Poisson's ratio		0.33
Third order elastic constants (GPa)	A	-320
	B	-200
	C	-190